iJRASET
International Journal For Research in Applied Science and Engineering Technology

# INTERNATIONAL JOURNAL FOR RESEARCH

IN APPLIED SCIENCE & ENGINEERING TECHNOLOGY

**Volume:** 11 **Issue:** X **Month of publication:** October 2023

**DOI:** https://doi.org/10.22214/ijraset.2023.56054

www.ijraset.com

Call: 08813907089 | E-mail ID: ijraset@gmail.com

International Journal for Research in Applied Science & Engineering Technology (IJRASET)
*ISSN: 2321-9653; IC Value: 45.98; SJ Impact Factor: 7.538*
*Volume 11 Issue X Oct 2023- Available at www.ijraset.com*

# Classification and Analysis of Solar X-ray Monitoring Data for Intensity Monitoring

Kashish Datta[1], Adityasinh Jadeja[2], Duttresh Sapra[3], Dr. Zankhana H. Shah[4]
*Birla Vishvakarma Mahavidyalaya, Mota Bazaar, Anand-388120, India*

***Abstract:*** ***Scientists have focused on solar flares because they are violent phenomena that take place on the Sun's surface and atmosphere and pose threats to the highly advanced civilization on Earth. Electromagnetic radiation from these eruptions primarily manifests as X-rays, UV light, and sporadically visible light. The energy released by these eruptions is equivalent to that of millions of atomic bombs. The beauty of auroras is enhanced but communication systems are disrupted by geomagnetic storms, which frequently accompany flares via coronal mass ejections (CMEs). Long-distance radio communication is hampered by ionospheric ionization caused by X-rays, and GPS navigation may become less precise, especially in high-latitude areas. Increased radiation levels during solar flares pose a concern to both astronaut safety and satellite operations. Geomagnetic disruptions pose a threat to electrical networks, which could result in widespread blackouts. Complex observatories like the Solar Dynamics Observatory (SDO) and the Solar and Heliospheric Observatory (SOHO) are used to predict and reduce the effects of solar flares. Classifying and analyzing solar flares precisely can assist determine their possible effects, which can range from modest interruptions brought on by Class C flares to major disruptions brought on by X-class flares. This study advances our knowledge of solar-terrestrial interactions and helps with space weather forecasting, both of which are essential in today's highly developed society.***

## I. INTRODUCTION

A solar flare is a compelling and explosive occurrence on the surface of the Sun and in the solar corona, or outer atmosphere, of the Sun. These flares, which are the result of intricate and dynamic interactions within the Sun's magnetic field, are closely linked to areas of extreme magnetic activity on the Sun, particularly sunspots. These astronomical events are categorized according to the amount of energy they produce, with an X-ray-heavy classification scheme. Flares fall into three categories: C-class, M-class, and X-class, with X-class being the most powerful and possibly damaging. For determining the relative strength and probable effects of solar flares, these classifications are essential [1].

It's hard to believe how much energy is unleashed during a solar flare; it frequently exceeds the total energy produced by millions of atomic bombs. Most of this energy is released as electromagnetic radiation, which has a diverse spectrum of wavelengths. Notably, solar flares produce a lot of X-rays, UV light, and occasionally even visible light. Solar flares' X-ray emissions have a number of significant impacts on both Earth and the space environment around it.

For instance, these X-rays might ionize the ionosphere of the Earth, which can absorb radio signals and interfere with long-distance communication. During solar flare episodes, GPS navigation systems can potentially make mistakes, especially in high-latitude areas where the impact is most noticeable [2, 3].

Solar flares are notable for increasing auroras, often known as the Northern and Southern Lights, and for having an impact on communication systems. When powerful solar flares intensify the interaction between the solar wind and Earth's magnetic field, these ethereal and enchanting displays become even more vivid [4].

Strong solar flares can have far-reaching and disruptive effects on technology, especially when they are accompanied by coronal mass ejections (CMEs). These occurrences have the potential to cause geomagnetic storms, which might harm transformers and electricity systems, resulting in widespread and protracted blackouts. Additionally, during solar flare events, satellite operations, including communication and navigation systems, are susceptible to disruption. Due to higher radiation exposure during these events, astronauts in space, such as those on the International Space Station (ISS), are at an increased risk, necessitating protective measures and, if possible, mission rescheduling. Advanced equipment like the Solar Dynamics Observatory (SDO) and the Solar and Heliospheric Observatory (SOHO) are used by space agencies and observatories to track and forecast solar flares. With the use of these observatories, researchers can monitor the Sun's activity in real-time and determine how solar flares can affect Earth and its technologically dependent culture [5].

 

The Carrington Event of 1859 is one of the most important solar flare incidents in human history. Operators experienced electric shocks as a result of this incident, and there were instances of telegraph equipment catching fire on its own. Surprisingly, it was accompanied by spectacular auroras that could be seen all the way down in the Caribbean. In the end, solar flares are dazzling, incredibly energetic, and intricate phenomena that arise from the Sun's corona. They result from complex magnetic field dynamics and produce a wide range of electromagnetic radiation, which has an effect on Earth's technology, communications, and space environment. The prediction of space weather and the mitigation of potential effects on our technologically interconnected and reliant world are of utmost importance, and ongoing research and monitoring of solar flares are essential [6-8].

The authors of this study article provide a detailed explanation of the project's objectives, approaches, results, and key implications. The study also investigates the complex technological elements of the web-based interface created to provide simple system access. Through this multifaceted analysis, the researchers want to shed light on the path to a deeper knowledge of solar flares and their spectrum of intensities, a goal that inevitably increases the domains of solar physics and the precision of space weather forecasting.

## II. EFFECT OF SOLAR FLARE ON EARTH

Solar flares have a wide-ranging and significant impact on Earth, affecting both its technological environment and the environment in space. Starting with geomagnetic storms, these impacts cover a wide range of fascinating and occasionally troublesome occurrences. Coronal mass ejections (CMEs), which are frequently accompanied by solar flares, can produce charged particles that can reach Earth and cause geomagnetic storms [9].

The Northern and Southern Lights, which are intensified auroras, are famed for appearing spectacularly during these storms. These natural light shows are mesmerizing to viewers all over the world during geomagnetic storms because they not only grow more bright but can also be seen at lower latitudes than usual. However, auroras' breathtaking beauty is contrasted with communication system outages. Geomagnetic storms cause signal absorption and interference in long-distance communication, particularly in the high-frequency (HF) radio band.

This interference has the potential to significantly affect crucial maritime and aviation operations, highlighting how crucial dependable communication is for coordination and safety. Additionally, because to mistakes in the signals used to determine global positioning, GPS navigational accuracy may suffer during these geomagnetic variations, which will have an impact on a number of industries that depend on accurate location data [10].

Additionally, the ionosphere, a vital component of the Earth's atmosphere, undergoes complicated alterations as a result of solar flares. The ionosphere is ionized by the high-energy X-rays and extreme ultraviolet (EUV) radiation that solar flares release, which causes dynamic changes in radio signal transmission.

A wide range of contemporary technologies depending on radio signals, from aviation and maritime operations to global telecommunications networks, are impacted by these ionospheric variations, making it difficult to maintain continuous and reliable communication across great distances [11].

Solar flares are a serious threat to spacecraft and satellites circling the Earth in the field of space technology. Sensitive electronic components may be harmed by the increased radiation levels that occur during solar flare events, which could jeopardize the durability and functionality of these priceless space assets. Furthermore, there is a real concern about how vulnerable electrical grids are. Strong geomagnetic currents could be generated within power transmission lines by particularly intense solar flares, especially when they interact with CMEs. This susceptibility to geomagnetic disturbances puts transformers and other essential parts of power grids at serious risk, boosting the possibility of major blackouts and interruptions to regular societal operations [12].

Another crucial factor to take into account during solar flare events is astronaut safety, since increased radiation levels in space pose serious threats to those in orbit, especially those on board the International Space Station (ISS). To reduce the potential health effects on astronauts working in the harsh space environment, safety precautions must be carefully designed and carried out.

Last but not least, solar flares have the potential to have a significant impact on a variety of technology-dependent systems, such as navigation, telecommunications, and aviation. For instance, in order to avoid flying over polar regions during geomagnetic storms and maintain passenger and crew safety, airlines may need to reevaluate their flight plans [13]. Solar flares are extremely interesting to the scientific community despite their potential for disruption. Understanding the Sun's behavior, the complex dynamics of its magnetic fields, and the broader topic of space weather requires a thorough understanding of solar flares. This knowledge is crucial for improving space weather forecasting capabilities and creating mitigation plans for solar flares' possible effects on our increasingly technologically advanced and interconnected world [14].

## III. LITERATURE REVIEW

Numerous statistical analyses of solar flares have been conducted since the discovery of flares by Carrington and Hodgson in 1859. Numerous studies have examined the temporal and spatial distributions of solar flares, the ionospheric disturbance brought on by solar flares, and the relationship between solar flares and certain solar activity parameters [15-18].

The correlation between solar flares and other solar radiation parameters (X-ray flux, EUV flux, sunspot numbers, etc.) has been researched by some scientists. Le et al. (2011) examined the variational properties of X-ray and EUV flux during the flare and the relationship between them using Xray flux at 0.1-0.8 nm and EUV flux at 26-34 nm generated by X, M, and C class flares. The findings indicate that from C to X class flares, the EUV amplification does not linearly increase with X-ray output. Only 0.66, 0.58, and 0.54, respectively, are the correlation coefficients between increases in X-ray and EUV flux during X, M, and C class flares [19]. The association between the sudden increase in total electron content (SITEC), X-ray flux at 0.1-0.8 nm, EUV flux at 0.1-50 nm, and EUV flux at 26-34 nm was statistically analyzed by Zhang et al. (2011). When compared to X-ray flux at 0.1-0.8 and EUV flux at 0.1-50 nm, they discovered that SITEC is better correlated with EUV flux at 26-34 nm [20]. According to Temmer et al. (2001), the correlation coefficient between the number of sunspots and the total number of monthly flares from January 1975 to December 1999 is 0.93 [21].

A lot of methods and attempts to develop an accurate flare-prediction system have been put forth. The Space Environment Center (SEC) at the National Oceanic and Atmospheric Administration (NOAA) implemented THEO (McIntosh, 1990), an expert system combining arbitrary judgments and statistical correlations, in 1987. This approach makes predictions for the occurrence of different solar-flare classes using a variety of sunspot and magnetic-field properties. Using the average flare rate for each human-observed McIntosh sunspot classification and Poisson statistics to determine the flare probability for each classification, Gallagher, Moon, and Wang and SolarMonitor (2002) developed a linear-prediction method. The properties of active regions and sunspot groups were determined using both linear statistical methods and non-linear prediction techniques, and later systems combined elements of both of these [22-24].

Numerous writers have conducted linear statistical studies in an effort to anticipate flares by determining the magnetic characteristics of the active zone that are most closely related to flare activity. Cui et al. (2006) used sigmoid analysis to examine the active-region maximum horizontal gradient, the length of the neutral lines, and the quantity of unique points using line-of-sight magnetograms. They discovered that even though there were strong correlations between these traits and flares, flares were not reliably predicted by these traits [25]. The mean value of spatial magnetic gradients along strong-gradient magnetic neutral lines, the length of strong-gradient magnetic neutral lines, and the total magnetic energy all showed a positive link with flaring, according to Jing et al. (2006). y. Leka and Barnes (2007) used linear discriminant analysis to calculate numerous properties from vector magnetograms. They discovered that the best methods for predicting flares of the C-class and higher range were total magnetic flux, total vertical currents, and measures of the magnetic shear, whereas flares of the M-class and higher range were best predicted using surplus photospheric magnetic energy [26].

Other research use substantial samples of defined active-region and sunspot group observations to train decision-making systems utilizing sophisticated non-linear learning techniques. Automated Solar Activity Prediction (ASAP), a machine learning-based hybrid method Colak and Qahwaji devised in 2009, uses measurements of sunspot area and automated McIntosh classifications. Machine learning was applied by Yu et al. (2009, 2010a, 2010b) to neutral-line parameters extracted from magnetograms [27]. The techniques used by Song et al. (2008) were integrated with machine learning by Yuan et al. (2010) [28, 29].

The temporal characteristics of solar flares have been the subject of various statistical investigations. In order to compare the flares' rise time and decay time, Pearce et al. (1993) proposed the asymmetry index of solar flare occurrences, which was used to characterize the asymmetry of the flares' evolution time. They discovered that, when this index was applied to the hard X-ray flare events between 1980 and 1985, the asymmetry of the flares was not immediately apparent but that the decay duration was longer than the rising time [30]. This is in contrast to the findings of Temmer et al. (2001), who examined Hα-flare events that occurred between 1975 and 1999 and found that there was a considerable asymmetry between the flare events' rise duration and decay time, with the decay time lasting roughly 1.5 times longer than the rise time [31]. The duration, rising time, and decay time of the flare episodes that occurred between 1976 and 2000 were statistically analyzed by Veronig et al. in 2002 [32]. The findings indicate that the entire flare duration is concentrated around 12 minutes, and that as the flare important class increases, so do the flare duration, rise time, and decay time. Joshi et al. (2010) came to the same conclusion and discovered that this phenomena is more evident for SCs 21 and 22's duration and decay time, whereas SC 23's is similar [33, 34].

 

International Journal for Research in Applied Science & Engineering Technology (IJRASET)
*ISSN: 2321-9653; IC Value: 45.98; SJ Impact Factor: 7.538*
*Volume 11 Issue X Oct 2023- Available at www.ijraset.com*

## IV. METHODOLOGY AND RESULTS

### *A. Data Capturing*

The measurement of photon flux, which counts the quantity of photons impacting a certain observational region over a specified period of time, allows one to quantify solar activity. The Indian Space Research Organization (ISRO) made data from the Solar X-Ray Monitor (XSM) on the Chandrayaan-2 satellite available for this study. The Solar X-Ray Monitor (XSM), which is outfitted with sensors and detectors designed to identify and gauge X-ray emissions during solar flare episodes, is an essential component of this research. These sensors record changes in X-ray intensity, enabling a thorough analysis of solar flare traits.

The systematic procedure of data acquisition involves the XSM continuously capturing X-ray emissions over a range of energy bands. Researchers and organizations interested in studying solar events can access this dataset thanks to ISRO's platform, which transmits it to Earth. Using information from the XSM improves the accuracy of solar flare analysis and facilitates cross-referencing with other solar observational tools and databases. Research on solar flares can study the intricacies of these solar phenomena and their implications for space weather forecasting and the resilience of terrestrial technology thanks to this data collection procedure, which is fundamental to the field.

### *B. Preprocessing*

Beginning with real data from the Chandrayaan-2 Orbiter's X-ray Solar Monitor (XSM) instrument, the empirical analysis is conducted. A thorough perspective of the X-ray emissions connected to solar flare episodes is provided by this dataset. A preprocessing procedure is carried out to guarantee data dependability. Raw data from the XSM is cleaned, calibrated, and formatted during preprocessing. This procedure aligns data temporally, removes noise, and corrects for instrument artifacts. Interpolation or extrapolation procedures are used to resolve missing or incorrect data, producing a polished dataset for analysis. Additionally, pertinent features such as X-ray flux levels, spectral properties, and temporal patterns are retrieved from the X-ray emissions data. These characteristics act as inputs for further analytical models and evaluations.

#### *1) Data Reading*

The 'Table' function offered by the Astropy library is used by the researchers to efficiently parse and ingest the lightcurve (LC) file at their disposal during the data analysis process. With the help of this powerful tool, complex astronomical data formats may be handled with ease, guaranteeing the data's correctness and integrity. After successfully loading the LC file, the researchers save this priceless dataset in a variable fittingly named "table" (fig. 1). Now that the dataset is available (fig. 2), the researchers start the critical process of locating and comprehending the different columns inside the dataset. In the lightcurve data, each column reflects a different facet of solar activity. As it enables the extraction of essential data and the creation of hypotheses and research questions, this first step establishes the framework for the succeeding phases of data analysis. This painstaking technique guarantees that the analysis is not only thorough but also focused on certain areas of solar behavior, adding to the scope and accuracy of the research.

| TIME | RATE | ERROR | FRACEXP |
|---|---|---|---|
| s | ct / s | counts/s | |
| 120960000.41355762 | 342.6589 | 18.511047 | 1.0 |
| 120960001.41355762 | 352.1104 | 18.764605 | 1.0 |
| 120960002.41355762 | 332.3823 | 18.231354 | 1.0 |
| 120960003.41355762 | 352.8552 | 18.784441 | 1.0 |
| 120960004.41355762 | 348.38522 | 18.665081 | 1.0 |
| 120960005.41355762 | 327.17093 | 18.087868 | 1.0 |
| 120960006.41355762 | 359.28 | 18.954683 | 1.0 |
| 120960007.41355762 | 317.38943 | 17.815428 | 1.0 |
| 120960008.41355762 | 326.1795 | 18.06044 | 1.0 |
| 120960009.41355762 | 324.0108 | 18.0003 | 1.0 |
| ... | ... | ... | ... |
| 121046389.41355762 | 649.55444 | 25.486359 | 1.0 |
| 121046390.41355762 | 674.07776 | 25.963007 | 1.0 |
| 121046391.41355762 | 590.47626 | 24.299717 | 1.0 |
| 121046392.41355762 | 678.0775 | 26.03992 | 1.0 |
| 121046393.41355762 | 662.1182 | 25.731659 | 1.0 |
| 121046394.41355762 | 629.2103 | 25.084064 | 1.0 |
| 121046395.41355762 | 628.4547 | 25.068998 | 1.0 |
| 121046396.41355762 | 615.2298 | 24.803825 | 1.0 |
| 121046397.41355762 | 578.09766 | 24.043661 | 1.0 |
| 121046398.41355762 | 645.4579 | 25.405863 | 1.0 |

Length = 46342 rows

Figure 1: Data Representation

 

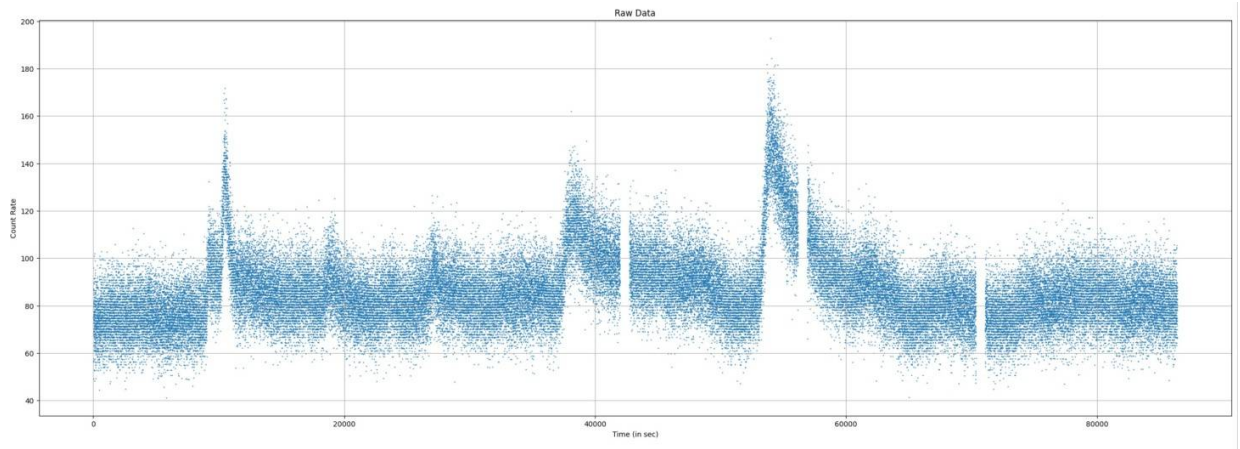


Figure 2: Raw Data

*2) Data Segmentation*

The authors start a segmentation method to improve the continuous data's quality. Each observation in our dataset typically has a one-second pause between adjacent data points. This innate temporal property directs our strategy for finding discontinuities in the data. We specifically identify these discontinuities as occurrences where successive measurements show a time lag that is more than one second.

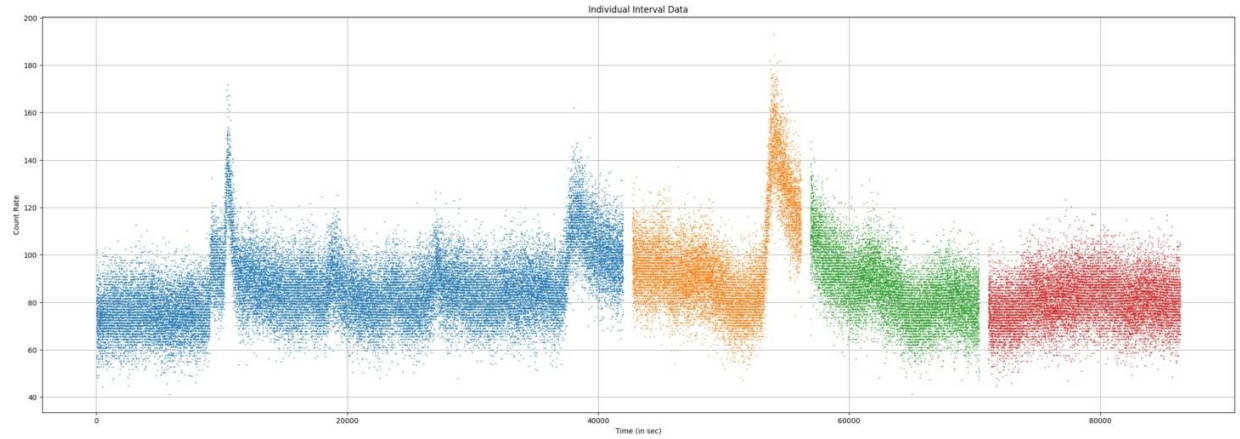


Figure 3: Information After Distinguishing Continuous Segments

It becomes clear through careful inspection that the data in this file naturally divides into four unique continuous segments. Figure 3 further supports this observation by clearly displaying three separate discontinuities. As a result, the researchers separate these continuous segments into four different arrays to enable more detailed analysis. Each of these arrays contains the data points that cover the interval of time between the start and end of a single segment. By successfully separating these continuous segments, our segmentation procedure creates the ideal environment for thorough analysis with little noise interference.

*3) Noise Reduction*

The researchers used a thorough strategy to try to reduce noise in the dataset. This method mainly consisted of replacing each of the 'n' successive data points with a single representative point, which was painstakingly calculated as the arithmetic mean of the segment in question. The researchers then carefully repeated the noise reduction method while moving a predetermined distance defined as "n/k" in a systematic way.

This iterative approach accomplishes two objectives. First and foremost, it successfully reduces the overall dataset's quantity of data points, methodically reducing noise interference. Second, it takes great care to maintain the vital elements of continuity and smoothness in the generated data, making sure that significant patterns and trends are maintained throughout the noise reduction process.

 

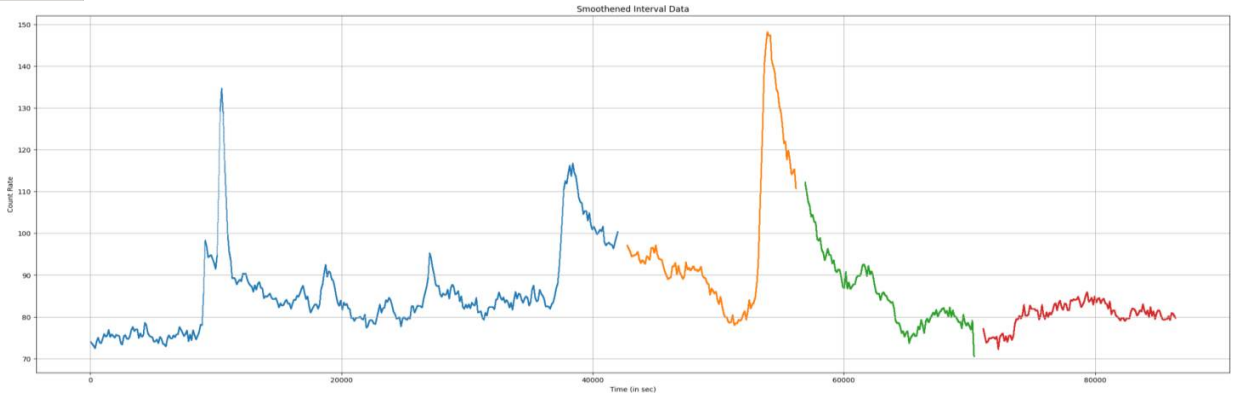


Figure 4: Smoothened Data

The researchers choose to display the resulting function in order to present a concrete and vivid portrayal of the results of this thorough noise reduction method. Plotting allows them to communicate the change of the dataset and to show how this methodical noise reduction procedure resulted in a more refined and smooth depiction. This image (fig. 4) not only helps to clarify how the dataset's noise has been reduced, but it also provides insightful information about the underlying patterns and trends in the data.

*4) Interpolation and data Harmonization*

The authors then went on to harmonize the dataset after carefully reducing noise and reconstructing parts of continuous data. This involved utilizing linear interpolation to precisely remove discontinuities. The outcome is a polished and continuous dataset that is thoughtfully presented in this work (fig. 5). A useful tool for thorough data visualization, a graphical representation showing the link between the final rate and final time has been incorporated to improve understanding.

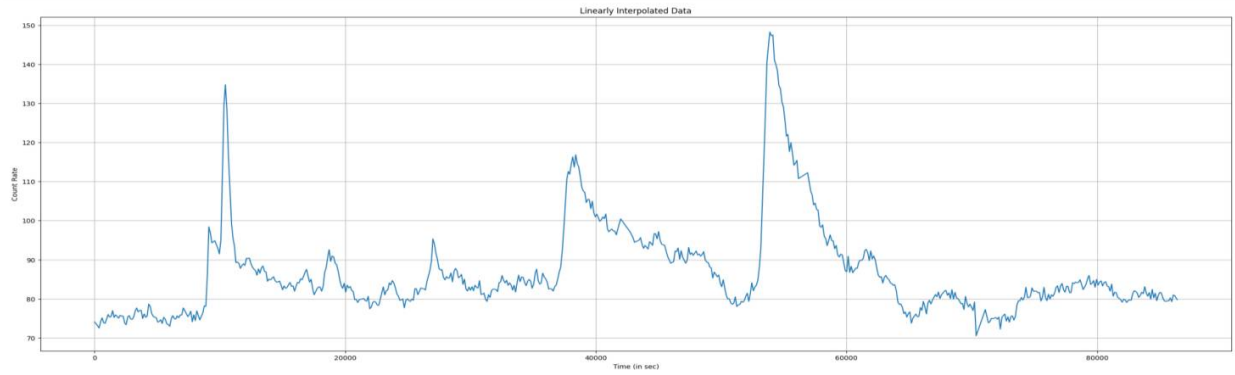


Figure 5: Final Pre-proposed Data

The researchers used interpolation to improve the quality of the data, reduce noise, and restore continuous segments. Discontinuities were purposefully eliminated through the methodical use of linear interpolation, producing a dataset that is both continuous and error-free. The study presents this harmonized, refined, and analysis-ready data. The relationship between the final rate and final time is deliberately represented graphically to help with comprehension and to aid in the depiction of important dataset dynamics.

*C. Detection*

The method used by the study team to identify solar flares is defined by a precise set of processes that are intended to guarantee the process's highest level of accuracy and dependability. The first step that the researchers concentrate on is Step 1: Finding Maxima in the dataset. Finding all maxima, which may be candidates for solar flare peaks, is the first stage in the process. The comparable minima, occurring right before each identified maximum, are carefully chosen in order to properly identify the beginning of a solar flare. Step 2: Initial Filtering is the next step. The researchers investigate solar flare properties based on Ascent Slope. Usually, the strength of solar flares increases quickly and then gradually decreases. The ascending slope must meet a particular standard in order to be classified as a solar flare, necessitating a large rise in photon count during this phase.

Step 3: Handling Noise and Minima Detection intelligently addresses potential noise in the data. The researchers consider scenarios in which minima could appear during the ascent phase of the flare, perhaps resulting in the identification of two flares rather than one. An extra filter is used to evaluate the temporal proximity of flare onset times and the size of the observed minima in order to counteract this. To maintain accuracy, start timings that are closely spaced apart and minima that are smaller in size are combined into a single flare.

Energy Threshold, Step 4-A crucial component of solar flare detection is filtering. While the flare's shape is important, its energy level is just as significant. The research team computes the mean peak count rate for all remaining potential flares to account for this. The investigation of flares with mean energies lower than this is halted because it is determined that they are too weak to be studied further. Finally, the identification process is completed by Step 5: Determining the End Point. It chooses a suitable minima, which often follows the flare peak. This marks the end of one flare and possibly the beginning of another. The research team creates a strong and complete framework for solar flare detection by carefully carrying out these rigorous stages. With this system, the possibility of false positives and interference from noise is kept to a minimum while relevant and scientifically valuable flare data are extracted (fig. 6).

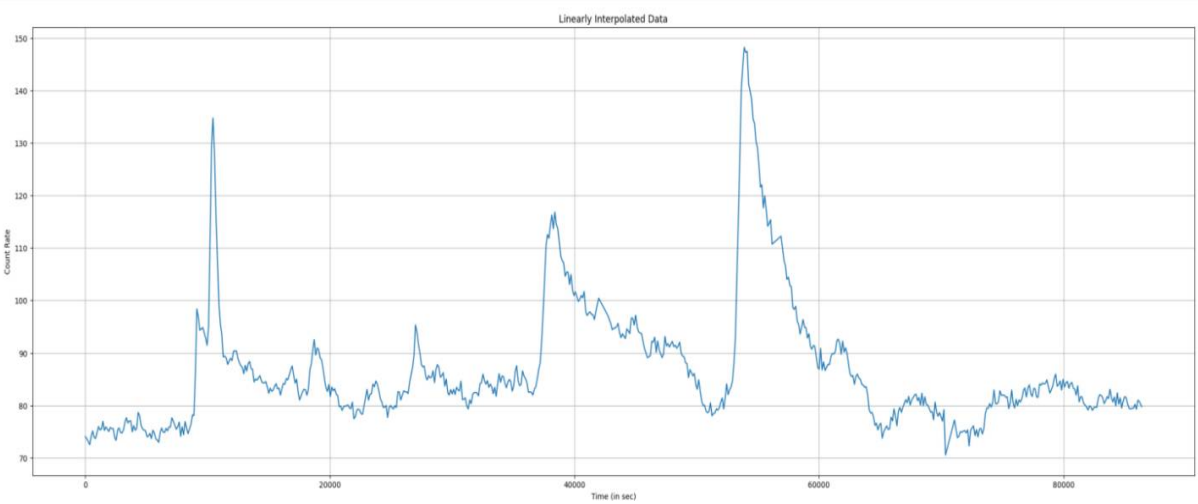


Figure 6: After Detecting the Peaks, Starts, and Ends of Each Solar Flare, the Final Data

*D. Modelling*

In the context of this study, the examination the following pair of functions is performed (fig. 7):

*1)* Gaussian Function: $f_1(t) = A \cdot e^{-(t-B)^2/C^2}$

*2)* Exponential Function: $f_2(t) = e^{-Dt}$

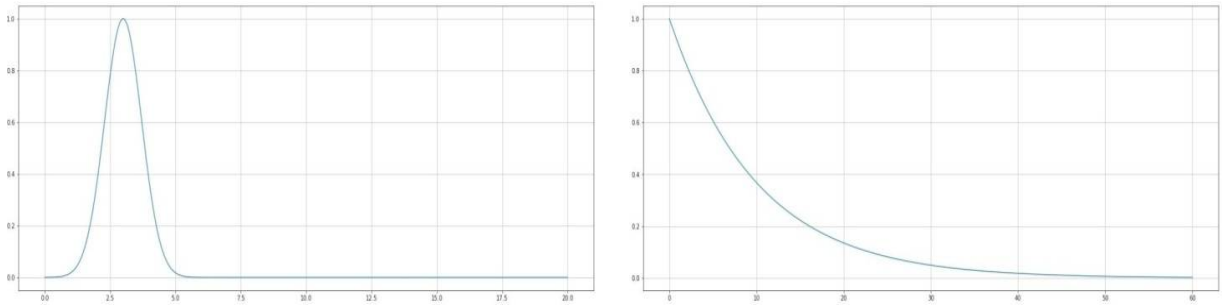

Figure 7: Function $f_1(t)$ and $f_2(t)$

Through the above-described convolution of the Gaussian and exponential functions, it is possible to successfully approximate a solar flare. The method used to calculate this convolution is as follows (fig. 8):

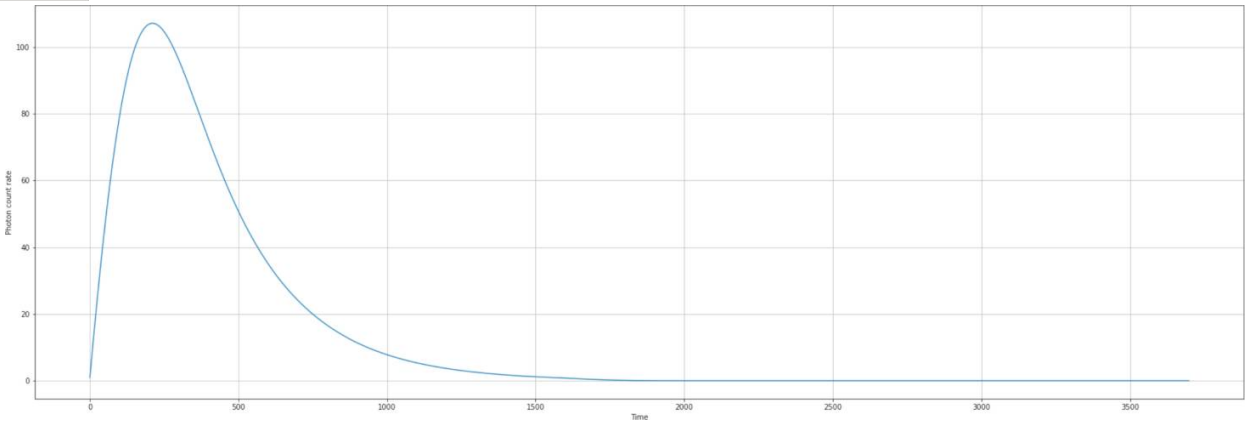


Figure 8: Elementary Flare Profile (EFP)

Empirically:

$$EFP(t) = \frac{\sqrt{\pi}}{2} ACe^{D(B-t)+\frac{C^2D^2}{2}} \left[\text{erf}\left(\frac{2B+C^2D^2}{2C}\right) - \text{erf}\left(\frac{2(B-t)+C^2D}{2}\right)\right] + Et + F \quad (1)$$

where the linear background radiation, $f_{bg}(t)$ is represented as:

$$f_{bg}(t) = Et + F \quad (2)$$

In the process of detecting solar flares, the researchers first pinpoint what appear to be the flare's beginning and end locations, which covers the time period during which they are certain that a single flare event has occurred. The ascending and descending phases (fig. 9) of the solar flare must be prolonged until they cross the actual background photon count for that day (the minimum photon count) in order to determine the exact times at which a flare genuinely begins and ends. Their modeling strategy is built on the Elementary Flare Profile (EFP) function, notwithstanding its complexity. They decided to model the rising and declining phases of the flare independently in order to reflect it appropriately. Specifically, a linear model is used for the rising phase. The EFP's characteristics, which show a sharp rise and considerable curvature especially near the apex, support this decision. As a result, it is discovered that a linear approximation offers an accurate depiction of the rising phase.

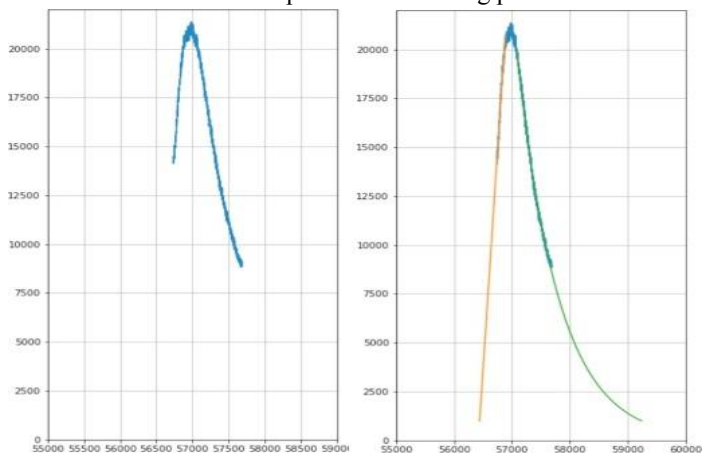

Figure 9: Modelling the Rise And Decay Phases

In contrast, the researchers use a model of the type $Ae^{-bt}$ for the decay phase. They began by thinking of a model with the parameter c, represented by the letter $Ae^{-bxc}$. Nevertheless, it was clear after extensive testing that c was set to 0.5 to get the best outcomes. The outcomes shown in their figures, where the fitting procedure produced an incredibly exact approximation of the decay phase, support this decision. The researchers are able to determine the precise seconds that correspond to the background photon count by utilizing the curves produced by this fitting procedure. They can accurately pinpoint the beginning and end of the solar flare event because to this precision, which raises the overall accuracy of their detection approach.

 

In the discipline of space science, knowing the exact start and end times of a solar flare occurrence is of utmost importance. The X-Ray Solar Monitor (XSM) and the Chandrayaan 2 Large Area Soft X-ray Spectrometer (CLASS), two important instruments on board the Chandrayaan-2 Orbiter, work together to demonstrate its significance. In order to detect solar flares, the XSM is primarily pointed at the Sun, whilst the CLASS sensor is concentrated on the lunar surface.

A notable occurrence during a solar flare outburst is the activation of the chemical elements present on the lunar surface, which results in detectable changes in their spectral signatures. It becomes crucial to precisely determine the start and end periods of the flare event, as inferred from the data acquired by XSM, in order to get important information into the composition and abundance of these active elements.

Its relevance in assisting the subsequent analysis of significant data acquired by the CLASS instrument highlights the crucial importance of getting this accurate temporal information. Researchers can gain a thorough knowledge of the flare-induced lunar surface activation by synchronizing the temporal bounds and comparing the observational data from both equipment. This unified strategy not only increases the mission's scientific significance but also significantly broadens our understanding of solar-terrestrial interactions.

### *E. Classification of Solar Flare*

They use the classification table (table 1) to group solar flares according to their peak photon count rate, which determines their peak flux:

Table 1: Classification of Solar Flare

| Class | Count Rate (s-1) | Flux (Wm-2) |
|---|---|---|
| A | N < 250 | X < 10-7 |
| B | 250 < N < 2500 | 10-7 < X < 10-6 |
| C | 2500 < N < 25000 | 10-6 < X < 10-5 |
| M | 25000 < N < 250000 | 10-5 < X < 10-4 |
| X | 250000 < N | 10-4 < X |

A Class C solar flare is normally thought of as being quite weak and does not typically pose a serious threat to Earth. An M-class flare, on the other hand, has the potential to cause modest radiation storms and transient radio blackouts in the polar areas, which might be problematic for astronauts in orbit. The X-class flares, known for their ability to produce protracted radiation storms that may imperil satellite performance, are the most potent of these events, though. The following image shows the relative sizes of Class C, M, and X flares.

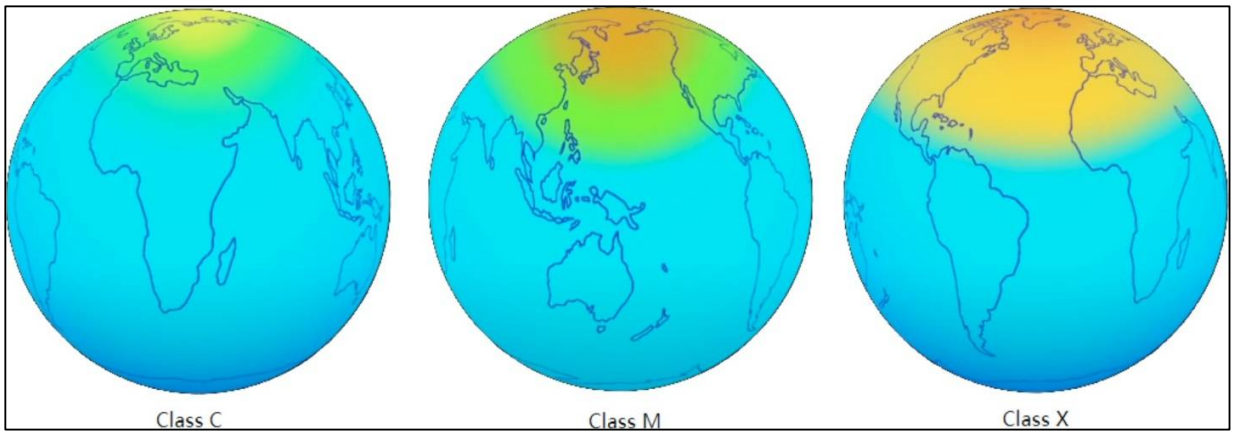


Figure 10: Relative Strengths of Different Classes

The table indicates that a solar flare that has a peak count rate of 1000 photons per second belongs to the Class B group. Solar flares belonging to this class can then be further separated into subclasses. For example, subclass B0 corresponds to a count rate of 250, whereas subclass B9.9 is roughly aligned with a count rate of 2499. The logarithmic scale has a uniform distribution of intermediate values. Consequently, the following is the general phrase for identifying the subclass of a flare with a peak count rate of x.

$$Subclass = 10log_{10}(\frac{x}{250}) \quad (3)$$

In the context of this discussion, the variable 'x' denotes the peak intensity of the solar flare, measured in the count rate. This specific case exemplifies

$$Subclass = 10log_{10}\left(\frac{1000}{250}\right) = 10log_{10}(4) \approx 6.02 \quad (4)$$

According to the computation of its subclass, the in question solar flare can be categorized as Class B6.0.

## V. CONCLUSION

In conclusion, this study uses a multifaceted method to further our understanding of solar flares and their effects. A significant accomplishment is the accurate identification of solar flare event boundaries made possible by the cooperation between the Chandrayaan 2 Large Area Soft X-ray Spectrometer (CLASS) and the X-Ray Solar Monitor (XSM). We can now understand the temporal complexities of solar flare occurrences and their effects on the lunar surface thanks to this partnership.

Furthermore, our classification methodology offers a thorough framework for assessing these events by differentiating solar flares based on peak photon count rates and subclasses. This method gives us a comprehensive understanding of solar flare dynamics and their potential influence on our technological infrastructure, ranging from the comparatively benign Class C flares to the powerful X-class flares. Our toolkit for accurate flare characterization has been enriched by the addition of the subclass calculation formula, which is based on peak intensity. This method makes use of logarithmic scaling to provide a very accurate evaluation of solar flare events.

In conclusion, this study sheds light on the crucial importance of solar flare classification and analysis in the context of solar physics and space weather forecasting. It emphasizes how crucial complementary instrumentation, temporal accuracy, and subclassification are to expanding our understanding of solar-terrestrial interactions. These approaches have the potential to be extremely useful tools for both scientific study and real-world applications as we continue to explore the dynamic behavior of our Sun.

## REFERENCES

[1] E. Heino, Calibration and simulations of SIXS-P's response to energetic particles. M.Sc. Thesis, University of Turku (2016).
[2] Heyner et al., this issue (2020) D. Hovestadt, M. Hilchenbach, A. Bürgi et al., CELIAS—charge, element and isotope analysis system for SOHO. Sol. Phys. 162, 441 (1995).
[3] Huovelin, L. Alha, H. Andersson, T. Andersson, R. Browning, D. Drummond, B. Foing, M. Grande, K. Hämäläinen, J. Laukkanen, V. Lämsä, K. Muinonen, M. Murray, S. Nenonen, A. Salminen, H. Sipilä, I. Taylor, O. Vilhu, N. Waltham, M. Lopez-Jorkama, Planet. Space Sci. 50, 1345–1353 (2002)
[4] J. Huovelin, R. Vainio, H. Andersson et al., Solar Intensity X-ray and particle Spectrometer (SIXS). Planet. Space Sci. 58(1–2), 96–107 (2010).
[5] E.K.J. Kilpua, H.E.J. Koskinen, T.I. Pulkkinen, Coronal mass ejections and their sheath regions in interplanetary space. Living Rev. Sol. Phys. 14, 1 (2017).
[6] J.M. Laming, The FIP and inverse FIP effects in solar and stellar coronae. Living Rev. Sol. Phys. 12, 2 (2015).
[7] A. Lehtolainen, J. Huovelin, L. Alha, T. Tikkanen, Estimates of in-flight calibration source activities for the SIXS X-ray detectors on board BepiColombo. Nucl. Instrum. Methods Phys. Res., Sect. A 636(1), 48–60 (2011).
[8] A. Lehtolainen, L. Alha, J. Huovelin, R. Moissl, S. Korpela, H. Andersson, K. Kuparinen, Ground calibrations of the Solar Intensity X-ray Spectrometer (SIXS) on board BepiColombo. Nucl. Instrum. Methods Phys. Res., Sect. A 735, 496–511 (2014).
[9] R.P. Lin, B.R. Dennis, G.J. Hurford et al., The Reuven Ramaty High-Energy Solar Spectroscopic Imager (RHESSI). Sol. Phys. 210, 3 (2002)
[10] Moissl et al., this issue (2020) Murakami et al., this issue (2020) J. Näränen, H. Parviainen, K. Muinonen, K. Nygård, M. Peura, J. Carpenter, Icarus 198, 408–419 (2008)
[11] J. Näränen, J. Carpenter, H. Parviainen, K. Muinonen, G. Fraser, M. Peura, A. Kallonen, Adv. Space Res. 44, 313–322 (2009)
[12] S. Narendranath, P. Sreekumar, L. Alha, K. Sankarasubramanian, J.Huovelin.P.S. Athiray, Elemental abundances in the solar corona as measured by the X-ray solar monitor onboard Chandrayaan-1. Sol. Phys. 289(5), 1585–1595 (2014)
[13] P. Oleynik, R. Vainio, A. Punkkinen, O. Dudnik, J. Gieseler, H.-P. Hedman, H. Hietala, E. Hæggström, P. Niemelä, J. Peltonen, J. Praks, R. Punkkinen, T. Säntti, E. Valtonen, Calibration of RADMON radiation monitor onboard Aalto-1 CubeSat. Adv. Space Res. (2019).
[14] Orsini et al., this issue (2020) H. Parviainen, J. Näränen, K. Muinonen, J. Quant. Spectrosc. Radiat. Transf. 112, 1907–1918 (2011)
[15] Quémerais et al., this issue (2020) I.G. Richardson, Solar wind stream interaction regions throughout the heliosphere. Living Rev. Sol. Phys. 15, 1 (2018).
[16] Rothery et al., this issue (2020) Saito et al., this issue (2020) J.P. Santos, F. Parente, Y.-K. Kim, Cross sections for K-shell ionization of atoms by electron impact. J. Phys. B 36, 4211–4224 (2003).
[17] Ferguson, A. J.: Computer Programs for Assessment of Long Wavelength Radio Communications, Version 2.0, Technical document 3030, Space and Naval Warfare Systems Center, San Diego CA 92152-5001, 1998.
[18] Grubor, D., Suli c D., and Zigman, V.: Influence of solar X-ray flares on the Earth-ionosphere waveguide, Serb. Astron. J., 171, 29–35, 2005.

[19] McRae, M. W. and Thomson, N. R.: VLF phase and amplitude: daytime ionospheric parameters, J. Atmos. Sol.-Terr. Phys., 62, 609–618, 2000.
[20] McRae, M. W. and Thomson, N. R.: Solar flare induced ionospheric D-region enhancements from VLF phase and amplitude observations, J. Atmos. Sol.-Terr. Phys., 66, 77–87, 2004.
[21] Mitra, A. P.: Ionospheric Efects of Solar Flares, Astrophysics and space science library, 46, D. Reidel Publishing Company, Boston, 1974. Thomson, N. R.: Experimental daytime VLF ionospheric parameters, J. Atmos. Sol.-Terr. Phys., 55(2), 173–184, 1993.
[22] Hannan, M.A.; Lipu, M.S.H.; Ker, P.J.; Begum, R.A.; Agelidis, V.G.; Blaabjerg, F. Power electronics contribution to renewable energy conversion addressing emission reduction: Applications, issues, and recommendations. Appl. Energy 2019, 251, 113404.
[23] Sun, Y.; Zhao, Z.; Yang, M.; Jia, D.; Pei, W.; Xu, B. Research overview of energy storage in renewable energy power fluctuation mitigation. CSEE J. Power Energy Syst. 2019, 6, 160–173.
[24] Ayob, A.; Ansari, S.; Lipu, M.; Hussain, A.; Hanif, M. Monitoring Technologies for Multi-Sensor System based on Wireless Data Transmission Modules. Int. J. Adv. Trends Comput. Sci. Eng. 2020, 9, 39–44.
[25] Alper, A.; Oguz, O. The role of renewable energy consumption in economic growth: Evidence from asymmetric causality. Renew. Sustain. Energy Rev. 2016, 60, 953–959.
[26] Suman, S. Hybrid nuclear-renewable energy systems: A review. J. Clean. Prod. 2018, 181, 166–177.
[27] Zakaria, A.; Ismail, F.B.; Lipu, M.S.H.; Hannan, M.A. Uncertainty models for stochastic optimization in renewable energy applications. Renew. Energy 2020, 145, 1543–1571.
[28] Minh, P.V.; Quang, S.L.; Pham, M. Technical Economic Analysis of Photovoltaic-Powered Electric Vehicle Charging Stations under Different Solar Irradiation Conditions in Vietnam. Sustainability 2021, 13, 3528.
[29] Alsadi, S.Y.; Nassar, Y.F. Estimation of Solar Irradiance on Solar Fields: An Analytical Approach and Experimental Results. IEEE Trans. Sustain. Energy 2017, 8, 1601–1608.
[30] Awasthi, A.; Kumar, A.; Murali Manohar, S.R.; Dondariya, C.; Shukla, K.N.; Porwal, D.; Richhariya, G. Review on sun tracking technology in solar PV system. Energy Rep. 2020, 6, 392–405.
[31] Zurita, A.; Castillejo-Cuberos, A.; García, M.; Mata-Torres, C.; Simsek, Y.; García, R.; Antonanzas-Torres, F.; Escobar, R.A. State of the art and future prospects for solar PV development in Chile. Renew. Sustain. Energy Rev. 2018, 92, 701–727.
[32] Mesloub, A.; Ghosh, A.; Touahmia, M. Performance Analysis of Photovoltaic Integrated Shading Devices (PVSDs) and Semi-Transparent Photovoltaic (STPV) Devices Retrofitted to a Prototype Office Building in a Hot Desert Climate. Sustainability 2020, 12, 10145.
[33] Future of Deployment, Investment, Technology, Grid Integration and Socio-Economic Aspects; International Renewable Energy Agency: Abu Dhabi, United Arab Emirates, 2019.
[34] Padmanathan, K.; Govindarajan, U.; Ramachandaramurthy, V.K. Multiple Criteria Decision Making (MCDM) Based Economic Analysis of Solar PV System with Respect to Performance Investigation for Indian Market. Sustainability 2017, 2012, 1–19.

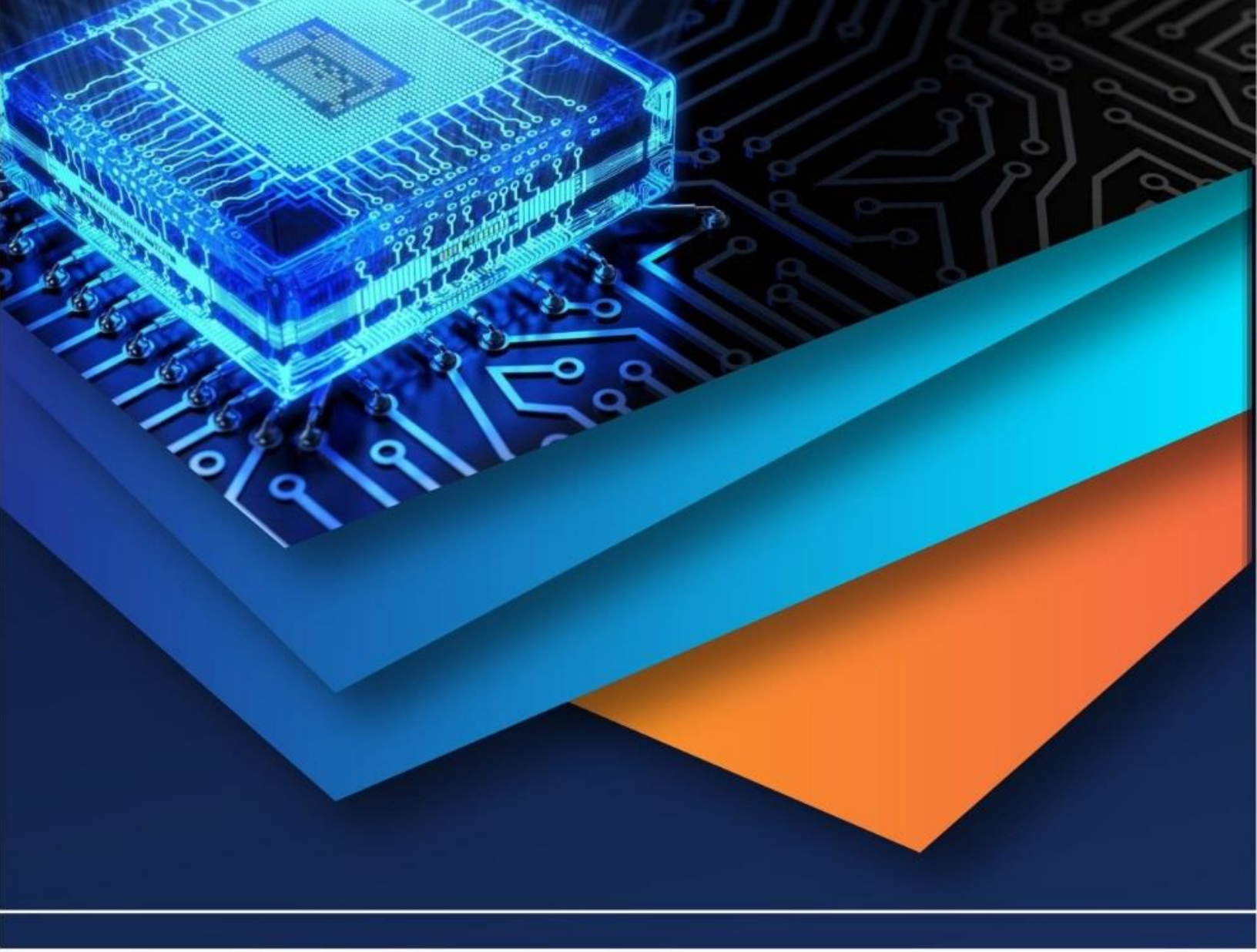

10.22214/IJRASET

45.98

IMPACT FACTOR: 7.129

IMPACT FACTOR: 7.429

# INTERNATIONAL JOURNAL FOR RESEARCH

IN APPLIED SCIENCE & ENGINEERING TECHNOLOGY